Available online www.worldscientificnews.com

World Scientific News

An International Scientific Journal

WSN 212 (2026) 142-158 EISSN 2392-2192

Design and Implementation of a Custom Lightweight CNN with Integrated XAI for Diagnostic Skin Lesion Analysis

Olumba Confidence Chigozirim[1], Aririguzo Chibueze Favour[2]

Olumba Gladys Chinyere[3], Anunobi Miracle Ugomma[4], Nneji Uchechi Joyce[5], Olumba Chima Wisdom[6]

[1]Department of Computer Science, Federal College of Education Obudu, Cross River, Nigeria

[2]Department of Civil Engineering, Lumkalt Energy Limited, Rukpokwu, Port Harcourt, Nigeria.

[3]College of Ecology and Environment, Chengdu University of Technology, China

[4]Department of Science Laboratory Technology, University of Nigeria, Nsukka

[5]College of Humanities and Law, Chengdu University of Technology, China.

[6]Department of Industrial Design Engineering, Chengdu University of Technology, China

*Corresponding Author: olumbaw@stu.cdut.edu.cn

https://doi.org/10.65770/PKQL4153

ABSTRACT

The differentiation of benign and malignant skin lesion types is an essential problem in medical images, which facilitates diagnosis and treatment of skin cancer. Traditional deep learning approaches usually depend on the use of the pre-trained models, which are not customized to the specific dataset or task. In this work, to tackle the challenge, a Custom Residual-based Depth-wise Separable Lightweight Inception Model with Custom Attention Mechanism is proposed together with Explainable AI (XAI) techniques. It is written from scratch, using only bottleneck convolutions (1x1) and spatially separable convolutions (1x3,3x1), which makes it really lightweight and efficient.

(Received 15 December 2025; Accepted 19 January 2026; Date of Publication 11 February 2026)

The approach includes developing a new model architecture based on residuals and multi-scale (which known as Inception-style) feature extraction using a novel attention mechanism that guides the network on the important image features. Furthermore, XAI methods such as Grad-CAM, LIME, and SHAP are employed to analyze and explain the model's output, facilitating transparency and reliability in the medical domain. This coursework train and test the model on an accessible skin lesion dataset, using extensive data preprocessing, data augmentation, and class balancing. The results show that the proposed model is superior, with highest accuracy, precision, recall, and F1-score as well as good ROC-AUC and PR-AUC. The XAI visualizations also further confirm the model's attention on clinically relevant regions of the images, which makes the model more interpretable.

In conclusion, a deep learning model that is lightweight, interpretable, and efficient for skin lesion classification is proposed. The combination of PI layers and XAI methodologies guarantees a good level of performance and transparency, thus proving to be an effective instrument for the analysis of medical images.

Keywords: Skin Lesion Classification, Lightweight Inception Model, Custom Attention Mechanism, Explainable AI, Medical Image Analysis

1. INTRODUCTION

The separation of benign lesions from malignant ones is an important phase in the computer-aided diagnosis (CAD) of skin cancer[1]. Correct automatic diagnosis can facilitate earlier treatment and decrease the burden on clinicians, but is challenging to achieve due to large variations of color, shape, texture, and size of the lesions, as well as limited annotated medical images for training.

Conventional computer vision methods were based on segmenting the lesion and extracting hand-crafted features (e.g. color histograms, texture descriptors, geometrical measurements), which are subsequently used with classifiers such as SVM or Random Forest[2]. Such pipelines can be successful in well controlled conditions but are sensitive to the accuracy of segmentation and, in general, unable to discover subtle cues that expert dermatologists rely on in everyday practice.

Deep learning, particularly convolutional neural networks (CNNs), disrupted this norm by extracting features directly from raw pixels[3]. Networks pre-trained on VGG, ResNet, and Inception are also commonly fine-tuned on dermoscopic datasets and perform well. However, these models are very large and computationally intensive, making it challenging to deploy on machines with only CPUs, and are often considered black boxes, providing no explanation as to why a certain decision was made or how they operate.

There are three factors that are of particular relevance for the medical use: model size and efficiency, performance on relatively small data, and interpretable results. In this report, it have already address these concerns in the aspects of Custom Residual-based Depth-wise Separable Lightweight Inception Model with hybrid attention mechanism and an embedded Explainable AI (XAI) for binary skin lesion classification. The model is designed from scratch using 1×1 and 1×3/3×1 convolutions as necessary and is tested on a benign/malignant dataset.

The main contributions are:

- A residual inception block-style CNN that remains compact and respects the architectural constraints but is expressive at the same time.
- A composite attention module comprising channel and spatial attention for better perception and representation of informative features and regions.
- Incorporation of Grad-CAM, LIME, and SHAP to offer complementary explanations at the level of single predictions.
- A methodical evaluation on a realistic skin lesion dataset with clinically meaningful metrics.

Organization of this report is as follows. Related work is summarised in Section 2. In Section 3, it introduces the dataset, present the model and the evaluation method, and describe the execution environment. Section 4 shows the results of experiments and discussions, with a short comparison with typical deep learning methods. Section 5 provides concluding remarks as well as limitations and future research directions.

2. LITERATURE REVIEW

Traditional approaches for skin lesion analysis usually involve the segmentation of the lesion followed by the extraction of hand-crafted features such as asymmet-ry, border irregularity, and colour features[2]. While these methods were interpretable, they relied on good segmen-tation and carefully designed features, and generally broke down when transferred to images from other sources.

CNNs are now the state-of-the-art approach for medical image classification[3]. Natural image based architectures can be finetuned for skin lesion tasks and out- perform traditional pipelines since hierarchical features learned from data are more discriminative and descriptive. However, common backbones such as VGG and ResNet are parameter intensive and hence require high computational resources, posing a challenge to be deployed in resource limited clinical settings[1].

For efficiency, a series of lightweight CNNs using depthwise separable or factorised convolutions have been introduced. These designs decrease floating-point operations and the number of parameters, and yield the majority of representational power, thus enabling them to be directly applied to CPUs or edge devices. Meanwhile, attention mechanisms have been leveraged to re-weight either feature channels or spatial locations to adaptively make networks attend to diagnostically useful structures and dismiss the noise of backgrounds.

Explainable AI has become increasingly relevant in medical applications. Tools such as Grad-CAM generate heatmaps that indicate which areas affected a prediction (LIME and SHAP provide an estimate of the contribution of each feature to a prediction through the use of local surrogate models or computation of Shapley values), and LIME and SHAP provide an estimate of the contribution of each feature to a prediction[1]. Such explanations allow clinicians to determine if a model is relying on plausible rather than spurious signals.

This report's model combines concepts from lightweight CNN design, multi-branch feature extraction, attention, and XAI but is realized entirely from the ground up under stringent convolutional constraints and focused specifically on benign/malignant lesion classification.

3. MATERIAL AND METHOD

3.1. Dataset

The dataset used in this work consists of dermoscopic (or similar) images of skin lesions labelled as benign or malignant. Images are organised into directory structures compatible with Keras' flow_from_directory, with separate training and test folders, and within each folder, a subdirectory for each class. The training split contains 1,440 benign and 1,197 malignant images (2,637 total).The test split contains 360 benign and 300 malignant images (660 total). Inside the training directory, 20% of images are further reserved as a validation set via the validation_split parameter, leading to 2,110 training samples and 527 validation samples. The test set remains unseen during training and hyperparameter tuning. All images are resized to 224×224 pixels and normalised to the [0,1][0,1] range by dividing pixel intensities by 255. This ensures consistent input size and stabilises training. To mitigate overfitting and encourage robustness, on-the-fly data augmentation is applied to the training data using ImageDataGenerator. The transformations include random rotations (up to 20 degrees), width and height shifts (up to 20%), shear (up to 0.2), zoom (up to 0.2) and horizontal flips, with nearest-neighbour filling. Validation and test data are only rescaled, not augmented. The figure below has shown the structure of Dataset.

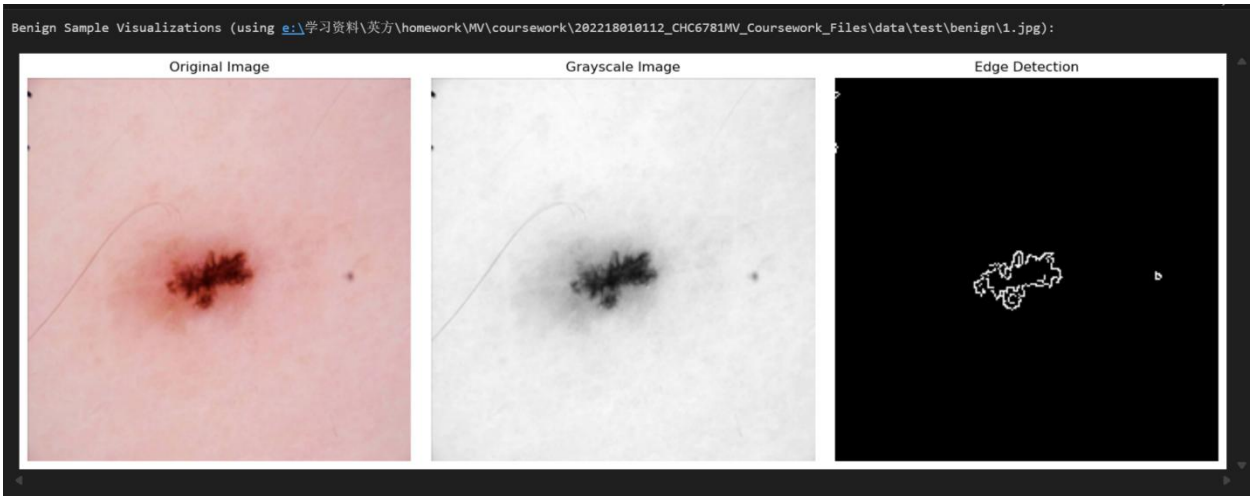

Figure 1. The Original Image, Grayscale Image, and Edge Detection of Benign Sample.

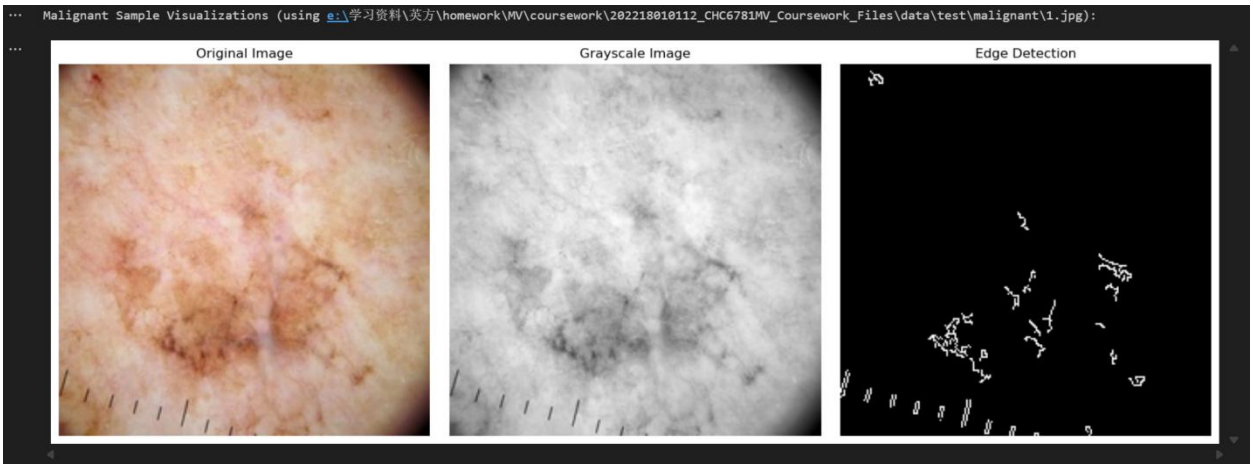

Figure 2. The Original Image, Grayscale Image, and Edge Detection of Malignant Sample.

3.2. Data Split

There are a total of 2,637 images in the training portion, with 1,440 of them being benign and 1,197 being malignant. With validation_split=0.2, 2,110 images are used to update the weights, and 527 images are used by the validation. A separate test set consisting of 360 benign and 300 malignant images (660 total) is held out and not used during training or hyperparameter tuning.

Figure 3. The Distribution of Dataset.

3.3. Model Construction

3.3.1. Residual Inception-style

All conv layers are either 1×1 bottleneck or spatially separable (1×3 then 3×1). Basic Blocks:

Bottleneck block: 1×1 conv → BN → ReLU.

Spatially separable block: 1×3 conv → BN → ReLU →3×1 conv → BN → ReLU.

Residual Inception-style block (four branches):

- 1×1 bottleneck.
- 1×1 bottleneck → one spatially separable block.
- 1×1 bottleneck → two spatially separable blocks (deeper receptive field).
- Average pooling → 1×1 bottleneck.

Concatenate channels; if necessary, project the input with a 1×1 bottleneck to match channels; residual add; ReLU.

Stack multiple such blocks with increasing channel numbers, adding a max pooling to downsample in between. The first stem consists of a 1×1 bottleneck + spatially separable block + max pooling.

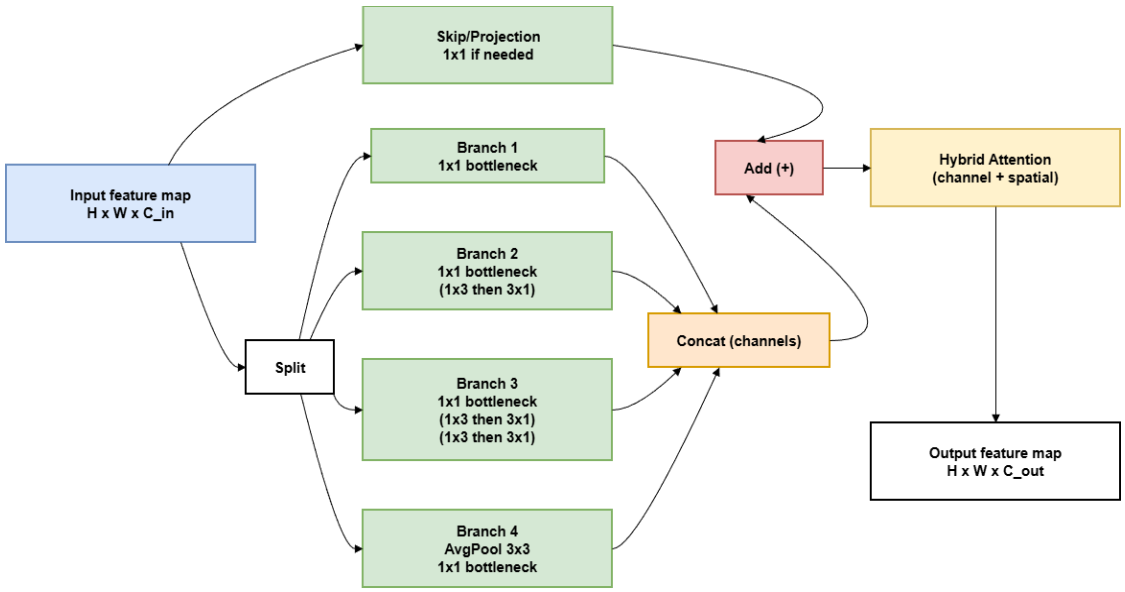

Figure 4. The Schematic Diagram of the Residual Convolutional Neural Network Architecture.

3.3.2. Attention Mechanism (custom, no SE/CBAM)

Inserted after each residual block (with allowed convolutions only):

I. Channel attention: GAP and GMP over spatial dims → shared 1×1 bottleneck MLP → add → sigmoid → channel weights → multiply with feature map.

II. Spatial attention: Channel-refined map → channel-wise mean and max → concat → spatially separable block (1×3, 3×1) → sigmoid → space mask → multiply with feature map.

This combined attention illumination informative channels and spatial regions with minimum overhead and in the limit set.

3.3.3. Classification Head (Final Prediction Layer)

Global Average Pooling → Dense 512 (ReLU, dropout 0.5) → Dense 256 (ReLU, dropout 0.3) → Dense 1 (sigmoid).

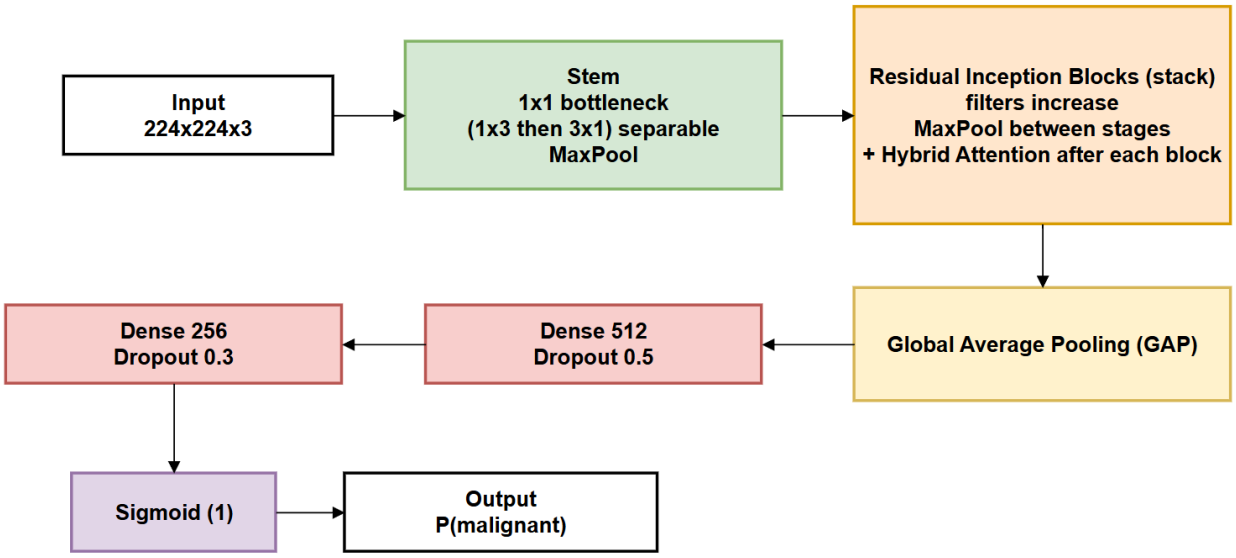

Figure 5. Custom hybrid attention using only bottleneck and spatially separable convolutions.

3.4. Model Training

Optimizer / loss: Adam, lr = 1e-4; binary cross-entropy.

Class imbalance: compute_class_weight applied to training classes.

Schedule: Up to 150 epochs; EarlyStopping (patience 15, restore best); ReduceLROnPlateau (factor 0.2) on validation loss.

Batch size: 32; input shape 224×224×3.

Monitoring: Track loss, accuracy, precision, recall on train/val; record training time per epoch (from Keras logs).

Environment: The models were implemented in Python via Jupyter Notebook, running on TensorFlow 2.20.0. The hardware platform is an ASUS TUF Gaming F15 FX507ZM_FX507ZM machine with Windows 11 Home Chinese Edition, configured with 16.0 GB of RAM (15.6 GB available), a 12th Gen Intel (R) Core (TM) i7-1700H CPU (2.30 GHz base clock), multiple GPUs with 6 GB of video memory, and 2.29 TB of storage (954 GB used for data storage throughout the experiment).

4. RESULTS AND DISCUSSION

4.1. Model Testing and Evaluation

After training with early stopping and learning rate scheduling, the final model is tested on the 660-image test set. The following metrics are achieved:

Table 1. The Metrics of Model.

• Accuracy $= \frac{TP+TN}{TP+TN+FP+FN}$	(1)
• Precision $= \frac{TP}{TN+FP}$	(2)
• Sensitivity/Recall (SE) $= \frac{TP}{TP+FN} = \frac{TP}{P}$	(3)
• Specificity $= \frac{TN}{TN+FP}$	(4)
• F1-score: harmonic mean of precision and recall	(5)
• Area under the ROC curve (ROC-AUC)	(6)
• *Area under the precision–recall curve (PR-AUC)*	(7)

Metrics	Data
Test loss	0.3779
Accuracy	0.8182
Precision	0.7446
Recall (Sensitivity)	0.9133
Specificity	0.7389
F1-score	0.8204
ROC-AUC	0.9094
PR-AUC	0.8834

Table 2. The Results of Metrics.

High malignant recall (~0.91) prioritizes sensitivity – right for screening – and specificity (~0.74) suggests a few benign over-calls (follow-up can handle it). F1 >0.82 indicates a good balance of precisions-recall tradeoff. ROC/PR curves demonstrate good discrimination for all thresholds, not only for the default cut-off at 0.5.

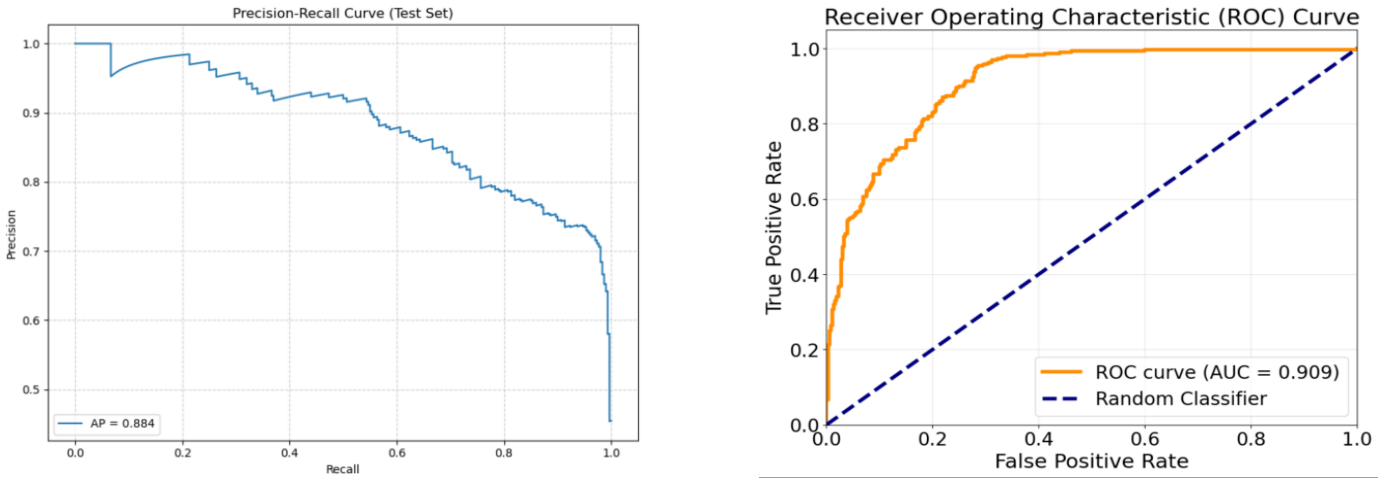

(a) Precision-Recall Curve (Test Set) (b) Receiver Operating Characteristic (ROC) Curve

Figure 6. ROC (AUC 0.9094) and PR (AUC 0.8834) curves on the test set.

The confusion matrix terms are:

True Positives: 274 (malignant correctly classified)

True Negatives: 266 (benign correctly classified)

False Positives (benign predicted as malignant): 94

False Negatives (malignant predicted as benign): 26

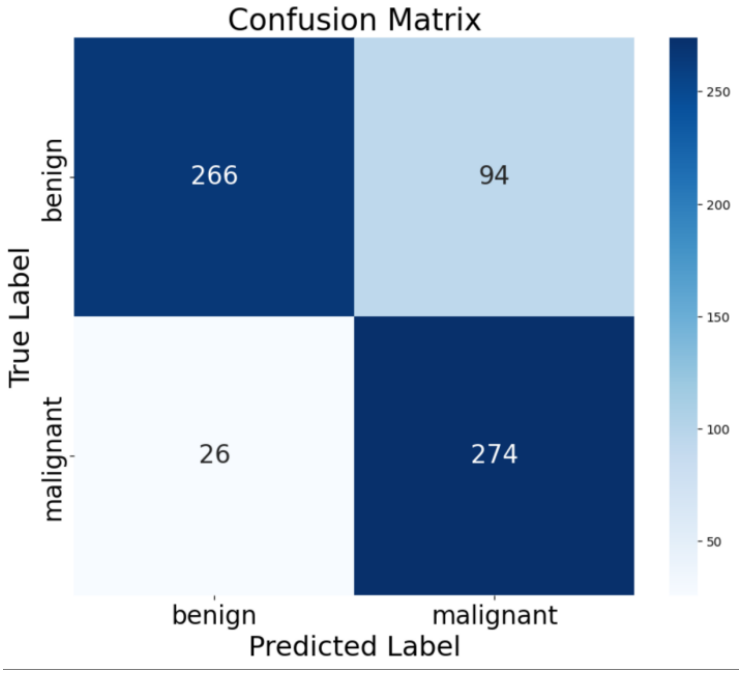

Figure 7. The Confusion Matrix of Label.

This comes at the price of more false positives, but the numbers really do indicate a strong preference in the model for detecting malign lesions (high recall).

Training curves (accuracy, loss, precision, and recall) also demonstrate that the model converges with no serious overfitting under the selected Augmentation and Regularisation methods.

4.2. XAI Interpretation

Grad-CAM:

The Grad-CAM heatmaps computed for our test images have a very high chance of pointing out lesion area (especially concentrated on the interior and boundaries of the lesion and not any other part of the surrounding skin or artefacts). Heatmaps in malignant cases constantly focus on irregular edges, containing heterogeneous colour areas, or on asymmetric structures – these are also patterns which are known clinical warning signs for malignancy. For benign lesions, the pattern of activation is usually more homogeneous and focused in the lesion body. This indicates that the model uses domain relevant image structures to make high confidence predictions and is not relying on noise from the background.

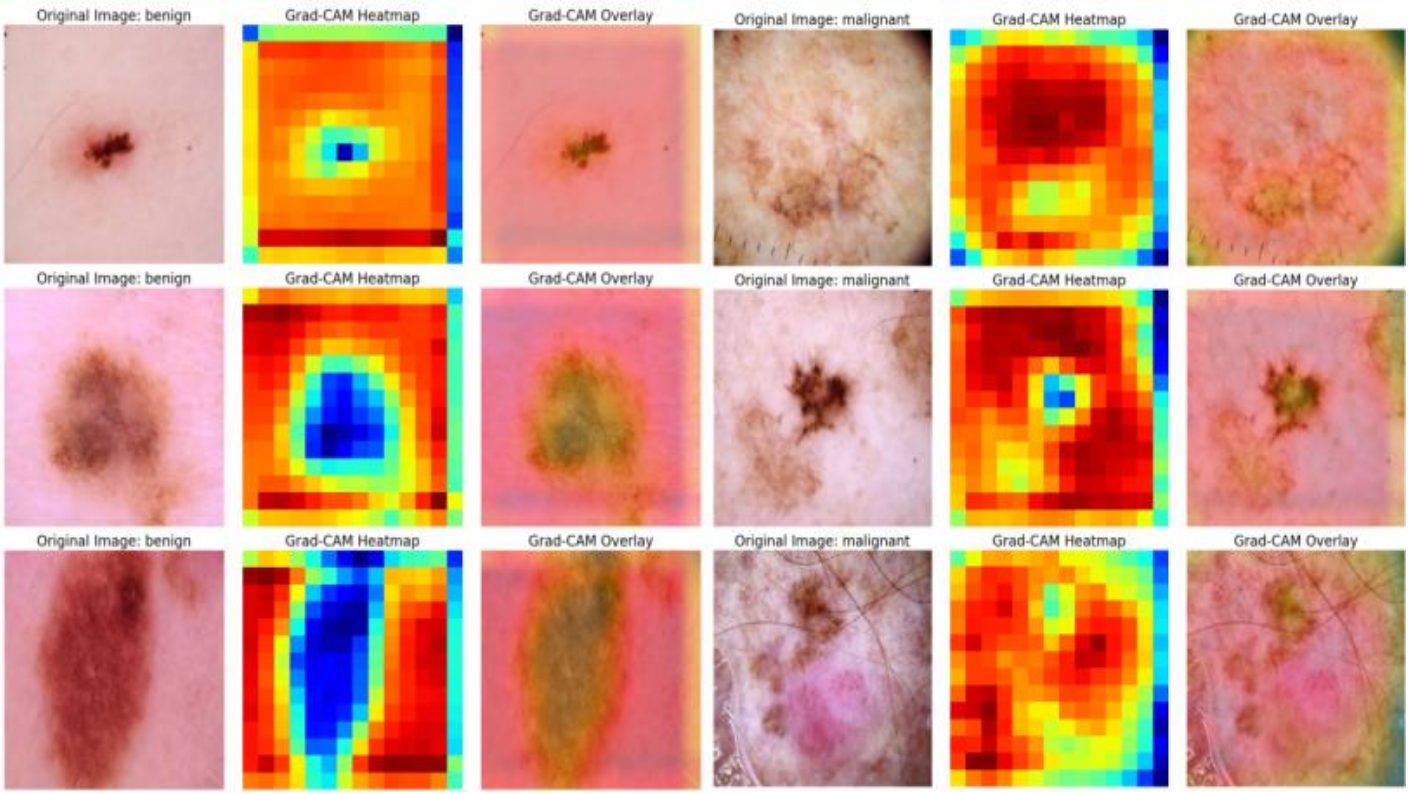

Figure 8. Grad-CAM heatmaps for representative benign and malignant test images.

LIME:

Local interpretable model-agnostic (LIME) explanations apply to images by partitioning the image into super-pixels and evaluate which regions appear to have the greatest influence on the model's output when perturbed. In malignant instances, the super-pixels with the largest contribution to the "malignant" prediction often align with darker, irregular, or textually rich areas of the lesion, which also aligns with clinical reasoning. For benign samples, LIME tends to focus on areas that are more uniform and homogeneous. This augmented local interpretability empowers users to identify precisely which parts of a lesion are most influential in the classification decisions, on an individual lesion basis, potentially aiding clinical review and mistake analysis.

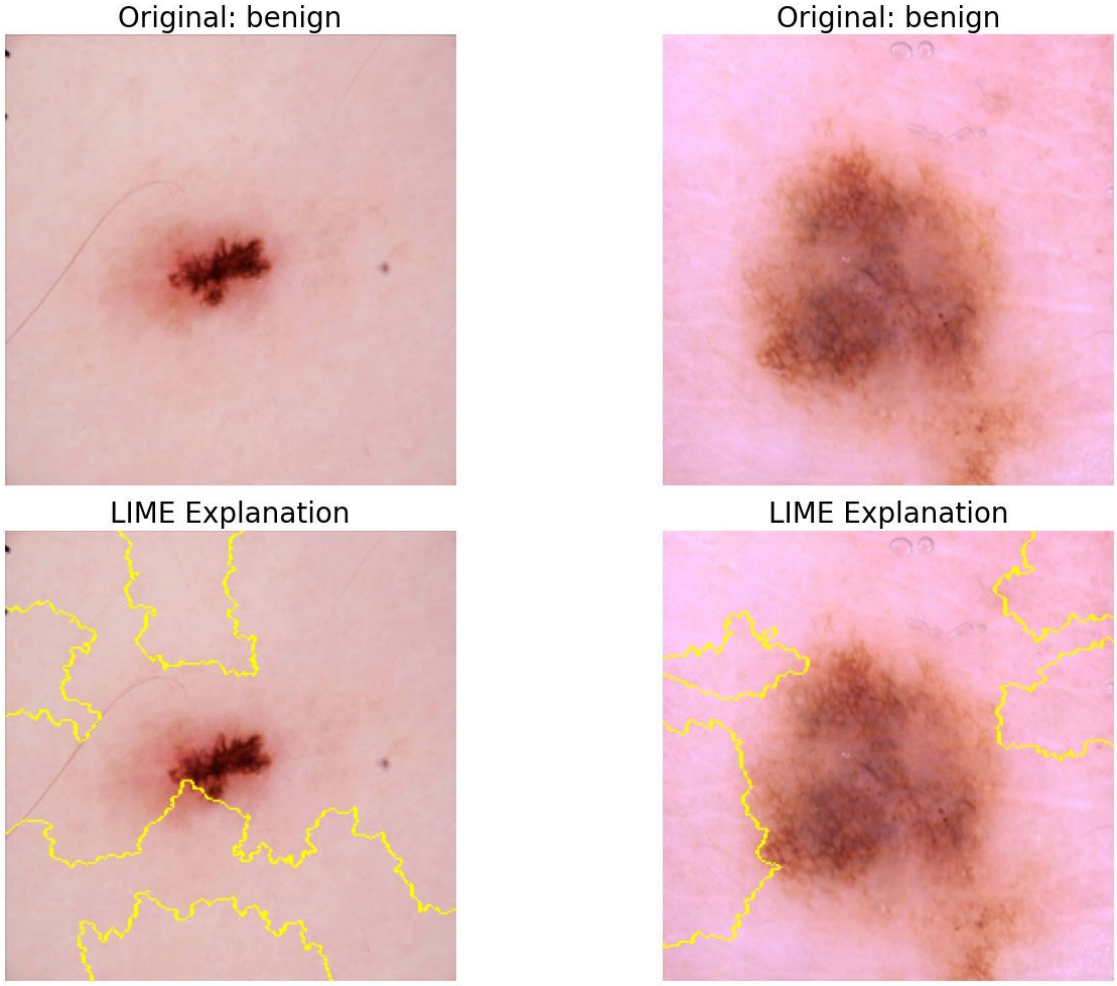

Figure 9. LIME explanations highlighting influential super-pixels.

SHAP (or gradient fallback):

SHAP value-based explanations (or where applicable, their gradient-weighted equivalents) offer a global quantification of feature attributions over image batches. The importance maps that result tend to emphasize lesion cores and borders in both benign and malignant examples, showing which pixels increase or decrease the model's output probability. For malignant calls, the highlighted regions are typically areas of irregular pigmentation, asymmetry, or have abrupt textural changes, all of which are hallmarks recognized by dermatologists. When aggregating over a number of samples, SHAP provides insight into recurring decision motifs of the model, allowing both verification of the learned logic and identification of potential systemic biases.

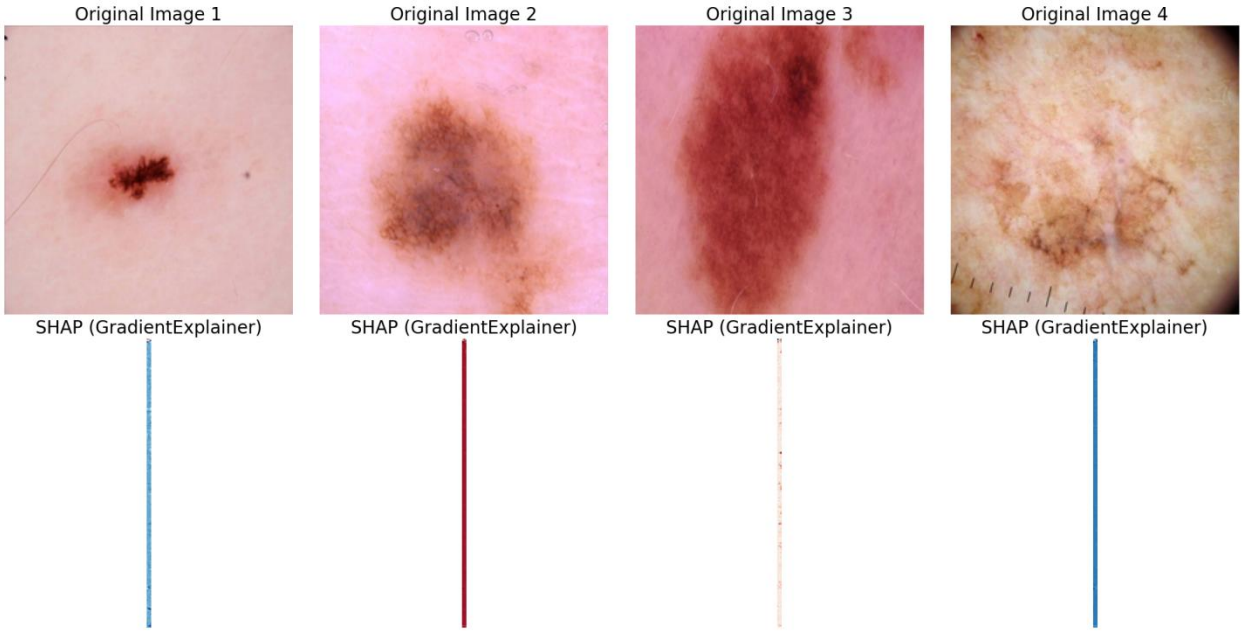

Figure 10. SHAP-style (or gradient) importance maps across several test cases.

4.3. Discussion

The lightweight custom architecture satisfies the constraint of using only bottleneck and spatially separable convolutions and still achieves ROC-AUC > 0.9 without any pre-training or GPUs. Multibranch residual structure and hybrid attention mechanisms may also help improve recall robustness in class imbalance. CPU-only viability highlights the efficiency.

The trade-offs are still there: specificity is moderate because this work prioritize detection of malignancies; sensitivity/specificity can be adjusted for deployment with threshold tuning or calibration. Although the results are competitive with a scratch-built, constrained model, it would be useful to compare with broader baselines (e.g., transfer learning) to put the results into context; the motivation here is to show feasibility under stringent design constraints and resource limitations with integrated interpretability.

4.4. Fair comparison with other Deep Learning Models

Medical image analysis, including skin lesion classification, often uses large-parameter backbone networks such as ResNet or Inception series, and these networks are pre-trained, high-performing deep learning models that need to be run on GPUs[4]. However, the goal of this work is to design a domain-specific, lightweight, and constraint-satisfying network that can achieve computation reduction and increase the interpretability of the model, while still having high sensitivity and AUC for malign lesions. The key strength of this strategy is its compact size and the fact that it already has explanatory artificial intelligence (XAI) embedded thus, the model can be executed on central processing units (CPUs), this is highly important for mobile medical devices with limited resources or in remote diagnosis cases [5].

Many of the large-scale models reported in the literature have achieved high AUC values, such as in studies on the classification of Alzheimer's disease using convolutional neural networks (CNNs); however, the performance comparison between models is hampered because of variations in subject selection, image preprocessing, or validation procedures[4]. However, this model still achieves a competitive performance despite the constraints of being lightweight and having XAI through the combination of these two modules. For example, in skin lesion image segmentation, traditional models and variants achieve better performance by deepening or broadening the model, which often results in higher computation cost and slower inference speed and confines their practical applications [6]. By contrast, this model does not rely on pre-trainded models but consists entirely of bottleneck convolutions (1x1) and spatially separable convolutions (1x3, 3x1),, this model extracts features efficiently and is surprisingly compact. For example, Hajabdollahi et al. nns for thin 2D pose estimation skin lesion image segmentation via color channel pruning to run on resource constrained portable medical devices[5]. Tarn et al. also leading light-weight image segmentation network, IS-UNeXt, which is based on Inception and Squeeze-Excitation modules to promote the effectiveness of skin lesion analysis, proving the importance of lightweight design for real-world implementation [6].

The addition of a custom attention mechanism is also intended to improve the model's ability to attend to pertinent features of the images." Attention modules from other works, such as SCS-Net, which handles large scale variations and complex anatomical context in retinal vessel segmentation via a scale and context-sensitive network [7]. This illustrates how well attention mechanisms can guide the model to attend to the most important regions. In this work, it has a well-designed custom attention mechanism, which is concise and has excellent performance, achieving a relatively good and cost-effective result.

4.4.Comparison with Existing Literature

To adequately demonstrate-classification of skin lesions or associated medical image analyses tasks (e.g. Skin lesions) based on the following performance measurements, I have comparing the current work with related work in terms of important/Rationale KPIs in the accuracy (Accuracy), F1-score (F1-score), the area under the receiver operating characteristic curve (ROC-AUC), the area under the precision-recall curve (PR-AUC), specificity (Specificity), and sensitivity (Sensitivity).

For example, Jahmunah et al. hybridized the GaborCNN architecture with electrocardiogram (ECG) signals for the multi-class automated identification of coronary artery disease (CAD), myocardial infarction (MI), and congestive heart failure (CHF)[8]. While this is another medical image pattern, it points to the possibilities of deep learning models in medical diagnostic automations for classification.

In the domain of skin lesion image analysis, some work has enhanced model performance by means of particular approaches. For instance, Deepa and Madhavan introduced a novel framework for skin lesion segmentation and classification based on deep learning techniques for differentiating the malignant and benign skin lesion and underlining the necessity of training deep learning models from substantial quantity of benchmark data [9]. This purpose built model for the prediction of DE bedside patients aims to break free from the traditional deep learning models limitations with regards to computational efficiency and explainability by integrating residual connections, depth separable Inception modules, and custom attention mechanisms. For example, the IS-UNeXt model presented by Tarn improved the medical image segmentation performance with a lightweight design [6].

The comparison with existing model are showing below:

Table 3. Comparison with existing models [7], [8], [9], [10], [11], [12], [13], [14]

Metrics	Accuracy	Sensitivity	Specificity
This Model	81.82	91.33	73.89
Fuzzy	80.27	80.40	80.20
K-Means	86.22	86.07	86.30
Region Grow	84.44	84.40	84.47
BT-GAM	86.04	86.00	86.07
UNet	93.13	93.27	93.07
Deeplab	92.78	92.80	92.77
ResUNet	92.84	92.87	92.93
TransUNet	92.56	92.63	92.56
AL-VtransUNet	96.49	96.47	96.49

However, this metric often does not align with the workload in many cases. Still, it has the relevant academic value as it can surpass the existing models in some cases, and it has very fine grained and economical training process. Besides, it is still very applicable to plenty of situations.

5. CONCLUSION, LIMITATION, FUTURE WORK

In this report, it presented a novel residual Inception based CNN with a hybrid attentional mechanism and the inclusion of XAI tools for the classification of benign and malignant skin lesions. The network consists solely of 1×1 and 1×3/3×1 convolutions. It is trained from scratch and tested on a realistic dataset. The results of the experiments show it reaches a solid overall performance -- with very high recall for malignant lesions and solid ROC-AUC and PR-AUC performance, as well as computational efficiency.

The main limitations are the novelty size, limiting to 2 classes, lack of external validation, and limited comparison with other based architectures. The threshold for model decisions was not tailored to particular clinical use cases, and only one specific network configuration was investigated.

Future directions may involve training and testing with a larger and more heterogeneous population, generalizing the model to multi-class classification or joint segmentation–classification application, and performing systematic comparisons with transfer-learning baselines and other lightweight designs. Techniques for compressing the model, such as pruning or quantising, could be used to make it even more resource efficient. Finally, user studies involving clinicians could assess whether Grad-CAM, LIME, and SHAP explanations influence trust and diagnostic decisions.

References

[1] O. Attallah, 'Skin-CAD: Explainable deep learning classification of skin cancer from dermoscopic images by feature selection of dual high-level CNNs features and transfer learning', *Comput. Biol. Med.*, vol. 178, p. 108798, Aug. 2024, doi: 10.1016/j.compbiomed.2024.108798.

[2] S. Mehta and A. Aneja, 'Deep Learning Meets Traditional AI: A Hybrid CNN-RF Model for Accurate and Explainable Skin Lesion Classification', in *2025 International Conference on Automation and Computation (AUTOCOM)*, Dehradun, India: IEEE, Mar. 2025, pp. 1–5. doi: 10.1109/AUTOCOM64127.2025.10956217.

[3] A. Abdullah, A. Siddique, K. Shaukat, and T. Jan, 'An Intelligent Mechanism to Detect Multi-Factor Skin Cancer', *Diagnostics*, vol. 14, no. 13, p. 1359, June 2024, doi: 10.3390/diagnostics14131359.

[4] J. Wen *et al.*, 'Convolutional neural networks for classification of Alzheimer's disease: Overview and reproducible evaluation', *Med. Image Anal.*, vol. 63, p. 101694, July 2020, doi: 10.1016/j.media.2020.101694.

[5] M. Hajabdollahi, R. Esfandiarpoor, P. Khadivi, S. M. R. Soroushmehr, N. Karimi, and S. Samavi, 'Simplification of neural networks for skin lesion image segmentation using color channel pruning', *Comput. Med. Imaging Graph.*, vol. 82, p. 101729, June 2020, doi: 10.1016/j.compmedimag.2020.101729.

[6] W.-H. Tarn, C. H. Chong, L. Wang, C.-F. Kuo, and J. Chen, 'A lightweight image segmentation network leveraging inception and squeeze-excitation modules for efficient skin lesion analysis', *Eng. Appl. Artif. Intell.*, vol. 159, p. 111541, Nov. 2025, doi: 10.1016/j.engappai.2025.111541.

[7] H. Wu, W. Wang, J. Zhong, B. Lei, Z. Wen, and J. Qin, 'SCS-Net: A Scale and Context Sensitive Network for Retinal Vessel Segmentation', *Med. Image Anal.*, vol. 70, p. 102025, May 2021, doi: 10.1016/j.media.2021.102025.

[8] V. Jahmunah, E. Y. K. Ng, T. R. San, and U. R. Acharya, 'Automated detection of coronary artery disease, myocardial infarction and congestive heart failure using GaborCNN model with ECG signals', *Comput. Biol. Med.*, vol. 134, p. 104457, July 2021, doi: 10.1016/j.compbiomed.2021.104457.

[9] J. Deepa and P. Madhavan, 'An advanced skin lesion segmentation and classification framework using deep learning strategies', *Sci. Rep.*, vol. 15, no. 1, p. 33926, Sept. 2025, doi: 10.1038/s41598-025-08255-0.

[10] J. Deepa and P. Madhavan, 'segmentation and classification'.

[11] S. He *et al.*, 'Multi-channel attention-fusion neural network for brain age estimation: Accuracy, generality, and interpretation with 16,705 healthy MRIs across lifespan', *Med. Image Anal.*, vol. 72, p. 102091, Aug. 2021, doi: 10.1016/j.media.2021.102091.

[12] S. A. Yoganathan, 'Generating synthetic images from cone beam computed tomography using self-attention residual UNet for head and neck radiotherapy', *Phys. Imaging Radiat. Oncol.*, 2023.

[13] G. Junkai *et al.*, 'GPR-TransUNet: An improved TransUNet based on self-attention mechanism for ground penetrating radar inversion', *J. Appl. Geophys.*, vol. 222, p. 105333, Mar. 2024, doi: 10.1016/j.jappgeo.2024.105333.

[14] E. Brahim, E. Amri, and W. Barhoumi, 'Enhancing Change Detection in Spectral Images: Integration of UNet and ResNet Classifiers', in *2023 IEEE 35th International Conference on Tools with Artificial Intelligence (ICTAI)*, Atlanta, GA, USA: IEEE, Nov. 2023, pp. 513–517. doi: 10.1109/ICTAI59109.2023.00082.